

Gradient-penalty stabilization of sharp and diffuse interface formulations in unfitted Nitsche finite element methods

Maxim Olshanskii^a, Jan-Phillip Bäcker^{b,*}, Dmitri Kuzmin^b

^a*Department of Mathematics, University of Houston
Houston, Texas 77204-3008, USA*

^b*Institute of Applied Mathematics (LS III), TU Dortmund University
Vogelpothsweg 87, D-44227 Dortmund, Germany*

Abstract

We introduce an unfitted Nitsche finite element method with a new ghost-penalty stabilization based on local projection of the solution gradient. The proposed ghost-penalty operator is straightforward to implement, ensures algebraic stability, provides an implicit extension of the solution beyond the physical domain, and stabilizes the numerical method for problems dominated by transport phenomena. This paper presents both a sharp interface version of the method and an alternative diffuse interface formulation designed to avoid integration over implicitly defined embedded surfaces. A complete numerical analysis of the sharp interface version is provided. The results of several numerical experiments support the theoretical analysis and illustrate the performance of both variants of the method.

Keywords: Elliptic interface problems; unfitted Nitsche finite element method; small cut cells; gradient-penalty stabilization; error analysis; level set; diffuse interface

1. Introduction

During the last two decades, immersed interface finite element methods have become an increasingly popular approach to solving complex problems with discontinuous material properties and moving boundaries [4]. The ability to perform simulations on a fixed (and often structured) mesh offers significant savings in terms of computational cost. However, the stability and accuracy of such geometrically unfitted formulations are strongly influenced by the numerical treatment of interface conditions. The unfitted Nitsche [12, 27] finite element method (FEM) and its stabilized counterparts, commonly known as cutFEM [8], are among the most successful discretization techniques of this type. The underlying weak forms include surface integrals that penalize violations of the interface conditions, as well as ghost penalty terms [5, 7, 21] that prevent ill-conditioning due to the presence of small cut cells. In

*Corresponding author

Email addresses: maolshanskiy@uh.edu (Maxim Olshanskii), jan-phillip.baecker@tu-dortmund.de (Jan-Phillip Bäcker), kuzmin@math.uni-dortmund.de (Dmitri Kuzmin)

many cases, optimal a priori error estimates and upper bounds for the condition number of the system matrix can be obtained for such unfitted finite element discretizations.

The practical implementation of cutFEM in existing codes presents certain challenges, including numerical integration over embedded and implicitly defined domains and interfaces, as well as the proper extension of the solution outside the physical domain. To address these challenges in the context of a stabilized unfitted Nitsche method, we:

- a) propose a versatile stabilization-extension operator for cutFEM approaches;
- b) analyze the stability and accuracy of the resulting finite element scheme;
- c) introduce and numerically study a diffuse interface version of our method.

In contrast to some other ghost penalties, our new gradient-penalty (GP) stabilization is parameter-free and easy to implement. It smoothly extends subdomain solutions beyond the physical domain into a buffer zone of a desired width and offers the additional benefit of stabilizing the convective terms, if present in the governing equation. The results of our theoretical studies confirm the favorable properties of our sharp interface GP method for an elliptic interface problem. In particular, we prove stability and derive a priori error estimates.

In the diffuse interface version, surface integrals are approximated by volume integrals using a regularized delta function, as in [13, 18, 19, 20]. The extension of data from the interface into its neighborhood is performed using Taylor expansions and the fast closest-point search algorithm developed in [20].

The remainder of this paper is organized as follows. In Section 2, we introduce a model problem and review the classical Nitsche finite element method. The new local GP stabilization operator is introduced in Section 3 in the sharp interface context. The diffuse interface formulation, presented in Section 4, eliminates the need for integration over sharp interfaces and cut cells. In Section 5, we analyze the GP stabilization technique. Numerical results are presented in Section 6. The convergence rates for test problems with smooth exact solutions are shown to be optimal. When the gradient is discontinuous across the interface, kinks in the solution profile are well captured. Finally, the main findings are summarized in Section 7.

2. An interface problem and unfitted Nitsche FE method

Let $\Omega \subset \mathbb{R}^d$, $d \in \{2, 3\}$ be a bounded Lipschitz domain, which is divided into two subdomains, Ω_1 and Ω_2 , by a smooth embedded interface Γ . For a function $v : \Omega \rightarrow \mathbb{R}$, its restriction to Ω_k , $k = 1, 2$ is denoted by v_k . The jump of v across Γ is denoted by $[[v]] = v_1 - v_2$. An average $\{v\} = \kappa_1 v_1 + \kappa_2 v_2$ is defined using a pair of weights $\kappa_1 \geq 0$ and $\kappa_2 \geq 0$ such that $\kappa_1 + \kappa_2 = 1$. The values of κ_1 and κ_2 may depend on $\mathbf{x} \in \Gamma$. The jump and average of a vector field $\mathbf{v}(\mathbf{x})$ are defined by $[[\mathbf{v}]] = (\mathbf{v}_1 - \mathbf{v}_2) \cdot \mathbf{n}$ and $\{\mathbf{v}\} = (\kappa_1 \mathbf{v}_1 + \kappa_2 \mathbf{v}_2) \cdot \mathbf{n}$, respectively.

We are interested in the following elliptic interface problem

$$-\nabla \cdot (\mu \nabla u) = f \quad \text{in } \Omega_k, \quad k = 1, 2, \quad (1a)$$

$$u = 0 \quad \text{on } \partial\Omega, \quad (1b)$$

$$[[u]] = 0 \quad \text{on } \Gamma, \quad (1c)$$

$$[[\mu \nabla u]] = 0 \quad \text{on } \Gamma, \quad (1d)$$

where

$$\mu = \begin{cases} \mu_1 & \text{in } \Omega_1, \\ \mu_2 & \text{in } \Omega_2, \end{cases}$$

$\mu_k > 0$ are constant rates of diffusive transport, and $f \in L^2(\Omega)$.

To build a numerical method for solving (1), we consider a regular conforming triangulation \mathcal{T}_h of Ω . For simplicity, we assume that the triangulation is fitted to the domain Ω in the sense that $\bigcup_{K \in \mathcal{T}_h} K = \bar{\Omega}$. For any $\delta \geq 0$, we define the sub-triangulations

$$\mathcal{T}_{h,k}(\delta) = \{K \in \mathcal{T}_h : \exists \mathbf{x} \in K \text{ s.t. } \text{dist}(\mathbf{x}, \Omega_k) \leq \delta\}, \quad k = 1, 2,$$

consisting of simplices that intersect a δ -neighborhood of Ω_k . The notation

$$\Omega_{h,k}(\delta) = \text{int}\left(\bigcup_{K \in \mathcal{T}_{h,k}(\delta)} K\right), \quad k = 1, 2$$

is used for the corresponding mesh-dependent domains. Note that $\Omega_k \subset \Omega_{h,k}(\delta)$ for all $\delta \geq 0$. In particular, for $\delta = 0$ the closure of $\Omega_{h,k}(0)$ consists of simplices that have a non-empty intersection with Ω_k .

Denote by $V_{h,k}(\delta)$ the finite element spaces of continuous piecewise affine functions with respect to $\mathcal{T}_{h,k}(\delta)$:

$$V_{h,k}(\delta) = \{v_h \in C(\Omega_{h,k}(\delta)) : v_h|_K \in P_1(K) \quad \forall K \in \mathcal{T}_{h,k}(\delta) \text{ and } v_h = 0 \text{ on } \partial\Omega \cap \partial\Omega_{h,k}\}.$$

The standard Nitsche finite element method for (1) reads as follows [12, 22]: Find $u_{h,k} \in V_{h,k}(0)$, $k = 1, 2$, such that

$$\begin{aligned} & \int_{\Omega_1} \mu_1 \nabla u_{h,1} \cdot \nabla w_{h,1} \, d\mathbf{x} + \int_{\Omega_2} \mu_2 \nabla u_{h,2} \cdot \nabla w_{h,2} \, d\mathbf{x} \\ & - \int_{\Gamma} [[u_h]] \{\mu \nabla w_h\} \, ds - \int_{\Gamma} \{\mu \nabla u_h\} [[w_h]] \, ds + \int_{\Gamma} \alpha [[u_h]] [[w_h]] \, ds \\ & = \int_{\Omega_1} f_1 w_{h,1} \, d\mathbf{x} + \int_{\Omega_2} f_2 w_{h,2} \, d\mathbf{x} \quad \forall w_{h,k} \in V_{h,k}(0), \quad k = 1, 2. \end{aligned} \quad (2)$$

Following [12], we define the averages using weights κ_1, κ_2 that are constant in each cell and represent the volume fractions of cut cells K from \mathcal{T}_h :

$$\kappa_k|_K = \frac{|K \cap \Omega_k|}{|K|}, \quad k = 1, 2. \quad (3)$$

The interior penalty parameter α depends on the local mesh size $h_K = \text{diam}(K)$: $\alpha|_K = \alpha_0 h_K^{-1}$ with a sufficiently large $\alpha_0 = O(1)$.

We define the bilinear and linear forms:

$$\begin{aligned} a_h(u, w) &:= \int_{\Omega_1} \mu_1 \nabla u_1 \cdot \nabla w_1 \, d\mathbf{x} + \int_{\Omega_2} \mu_2 \nabla u_2 \cdot \nabla w_2 \, d\mathbf{x} \\ &\quad - \int_{\Gamma} \llbracket u \rrbracket \{ \mu \nabla w \} \, ds - \int_{\Gamma} \{ \mu \nabla u \} \llbracket w \rrbracket \, ds + \int_{\Gamma} \alpha \llbracket u \rrbracket \llbracket w \rrbracket \, ds, \\ f(w) &:= \int_{\Omega_1} f_1 w_1 \, d\mathbf{x} + \int_{\Omega_2} f_2 w_2 \, d\mathbf{x}, \quad u, w \in H^1(\Omega_1) \times H^1(\Omega_2) \end{aligned}$$

to write (2) as the abstract problem

$$a(u_h, w_h) = f(w_h) \quad \forall w_h \in V_{h,1}(0) \times V_{h,2}(0). \quad (4)$$

Recalling the definitions of jumps and averages, we find the decomposition

$$\llbracket u_h \rrbracket \{ \mu \nabla w_h \} + \{ \mu \nabla u_h \} \llbracket w_h \rrbracket - \alpha \llbracket u_h \rrbracket \llbracket w_h \rrbracket = q_1(u_{h,1}, u_{h,2}, w_{h,1}) - q_2(u_{h,1}, u_{h,2}, w_{h,2}),$$

where

$$q_1(u_1, u_2, w_1) = (u_1 - u_2)(\kappa_1 \mu_1 \nabla w_1) \cdot \mathbf{n} + (\kappa_1 \mu_1 \nabla u_1 + \kappa_2 \mu_2 \nabla u_2) w_1 \cdot \mathbf{n} - \alpha(u_1 - u_2) w_1, \quad (5a)$$

$$q_2(u_1, u_2, w_2) = (u_2 - u_1)(\kappa_2 \mu_2 \nabla w_2) \cdot \mathbf{n} + (\kappa_1 \mu_1 \nabla u_1 + \kappa_2 \mu_2 \nabla u_2) w_2 \cdot \mathbf{n} + \alpha(u_2 - u_1) w_2. \quad (5b)$$

Using this notation, the finite element method (2) can be also written as the system of two coupled problems: Find $u_{h,k} \in V_{h,k}(0)$, $k = 1, 2$ such that

$$\int_{\Omega_1} \mu_1 \nabla u_{h,1} \cdot \nabla w_{h,1} \, d\mathbf{x} - \int_{\Gamma} q_1(u_{h,1}, u_{h,2}, w_{h,1}) \, ds = \int_{\Omega_1} f_1 w_{h,1} \, d\mathbf{x} \quad \forall w_{h,1} \in V_{h,1}(0), \quad (6a)$$

$$\int_{\Omega_2} \mu_2 \nabla u_{h,2} \cdot \nabla w_{h,2} \, d\mathbf{x} + \int_{\Gamma} q_2(u_{h,1}, u_{h,2}, w_{h,2}) \, ds = \int_{\Omega_2} f_2 w_{h,2} \, d\mathbf{x} \quad \forall w_{h,2} \in V_{h,2}(0). \quad (6b)$$

In what follows, we consider stabilized versions of (2). They can be restricted to the subdomains $\Omega_{h,1}(\delta)$ and $\Omega_{h,2}(\delta)$ similarly by using test functions $w_{h,1} \in V_{h,1}(\delta)$ and $w_{h,2} \in V_{h,2}(\delta)$, respectively.

3. Sharp interface GP formulation

Although well-posed, the finite element (FE) formulation (2) is prone to numerical instabilities. These instabilities arise from the potential inclusion of simplices in $\mathcal{T}_{h,k}(0)$ that intersect the ‘physical’ domain Ω_k only minimally. This stability issue was first addressed in [5] by introducing ghost penalty stabilization on simplices intersected by and adjacent to Γ . The approach proposed in [21] extends this penalization to a broader strip of elements within a distance $\delta > 0$ from Γ , as part of an implicit extension procedure for an Eulerian FE discretization. This formulation is particularly relevant to problems where the evolving interface Γ represents the boundary of a time-dependent embedded domain.

Let us now introduce a gradient-projection stabilization technique as an alternative to traditional ghost penalties in both roles: stabilizing against small cuts and providing a proper extension of $u_{h,k}$ to $\Omega_{h,k}(\delta)$ for $\delta > 0$. We define the *gradient-penalty* (GP) stabilization term

$$s_h(u, w) := \int_{\Omega_{h,1}(\delta)} \mu_1(\nabla u_1 - \mathbf{g}_{h,1}) \cdot \nabla w_1 \, d\mathbf{x} + \int_{\Omega_{h,2}(\delta)} \mu_2(\nabla u_2 - \mathbf{g}_{h,2}) \cdot \nabla w_2 \, d\mathbf{x} \quad (7)$$

with $u, w \in H^1(\Omega_{h,1}(\delta)) \times H^1(\Omega_{h,2}(\delta))$. The stabilization uses lumped-mass L^2 projections $\mathbf{g}_{h,k}$ of the (generally discontinuous) gradients $\nabla u_k \in (L^2(\Omega_{h,k}(\delta)))^d$ into the spaces $(V_{h,k}(\delta))^d$. Those $\mathbf{g}_{h,k}$ are computed locally as follows: Consider the nodal basis $\{\varphi_j\}_{j=1,\dots,N_{h,k}}$ in $(V_{h,k}(\delta))$, $N_{h,k} = \dim(V_{h,k}(\delta))$ and let

$$\mathbf{g}_{h,k} = \sum_{j=1}^{N_{h,k}} \mathbf{g}_{j,k} \varphi_j, \quad k = 1, 2.$$

Then the coefficients $\mathbf{g}_{j,k}$ are explicitly given by

$$\mathbf{g}_{j,k} = \frac{\int_{\Omega_{h,k}(\delta)} \varphi_j \nabla u_k \, d\mathbf{x}}{\int_{\Omega_{h,k}(\delta)} \varphi_j \, d\mathbf{x}}, \quad k = 1, 2. \quad (8)$$

Note that computing $\mathbf{g}_{j,k}$ involves integration only over triangles sharing the node \mathbf{x}_j , where $\varphi(\mathbf{x}_j) = 1$.

Adding the GP stabilization term (7) to the finite element formulation (4) results in the following sharp interface formulation: Find $u_{h,k} \in V_{h,k}(\delta)$, $k = 1, 2$, such that

$$a(u_h, w_h) + s_h(u_h, w_h) = f(w_h) \quad \forall w_h \in V_{h,1}(\delta) \times V_{h,2}(\delta). \quad (9)$$

Remark 1. Projection-based stabilization terms of the form (7) are widely used in FE formulations for convection-dominated transport problems [9, 10, 14, 15]. Consequently, their stabilizing effect can be naturally exploited in extensions of the proposed method to convection-diffusion equations (see Section 6.4 below for a numerical example). This is one of the reasons why we apply stabilization globally on $\Omega_{h,2}(\delta)$ rather than locally in a narrow strip around the interface. Another reason is the ease of implementation. While the ghost penalty term in unfitted FEMs is typically defined within a narrow band, we are not the first to consider a global definition of the ghost penalty; see, for example, [6, 23]. In particular, the recent report [24] demonstrated that defining the ghost penalty globally is necessary to ensure specific stability of the method in the case of moving interfaces.

4. Diffuse interface GP formulation

The calculation of integrals over cat elements and embedded interfaces in unfitted finite element discretizations of multidimensional interface problems is not always straightforward. To avoid the associated difficulties, we use the methodology developed in [20]. Assume that position of $\Gamma \subset \Omega$ is determined by a continuous level set function $\phi \in C(\bar{\Omega})$, which is positive in Ω_1 and negative in Ω_2 so that $\Gamma = \{\mathbf{x} \in \Omega : \phi(\mathbf{x}) = 0\}$. We assume that ϕ is smooth in an $O(1)$ neighborhood $\mathcal{O}(\Gamma)$

and $|\nabla\phi| \geq c > 0$ in $\mathcal{O}(\Gamma)$. Then the vector field $\mathbf{n} = -\frac{\nabla\phi}{|\nabla\phi|}$ defines an extended unit normal to Γ , pointing outward from Ω_1 . The methods employed in [13, 18, 19, 20, 29] approximate surface integrals over the interface Γ by volume integrals depending on a smoothed Dirac delta function $\delta_\epsilon(\phi)$. The small parameter $\epsilon > 0$ determines the quality of the approximation to $\delta(\phi) = \lim_{\epsilon \searrow 0} \delta_\epsilon(\phi)$. A typical definition of $\delta_\epsilon(\phi) \approx \delta(\phi)$ is given below.

For any $q \in C(\Omega)$, the integral $\int_\Gamma q(\mathbf{x}) \, ds$ can be approximated by $\int_\Omega q(\mathbf{x}) \delta_\epsilon(\phi) |\nabla\phi| \, d\mathbf{x}$. As explained in [20], the calculation of volume integrals that contain $\delta_\epsilon(\phi)$ requires an extension of the quantities defined on Γ into the interior of the two subdomains. To maintain the consistency of the weak form, we extend the interface values of functions and coefficients constantly in the normal direction determined by the gradient of the level set function ϕ . The efficient algorithm that we developed for this purpose can be found in [20]. Let \mathcal{E}_{cp} denote the closest point extension operator such that $\mathcal{E}_{\text{cp}}v(\mathbf{x}) = v(\mathbf{x}_\Gamma(\mathbf{x}))$, where \mathbf{x}_Γ is the closest point on Γ . Such extension of (5) is consistent with the jump conditions (1c) and (1d) of the interface problem in the sense that

$$\mathcal{E}_{\text{cp}}q_1(u_1, u_2, w_1) - \mathcal{E}_{\text{cp}}q_2(u_1, u_2, w_2) = 0 \quad \text{at } \mathbf{x} \in \Omega$$

if

$$\llbracket u \rrbracket = \llbracket \mu \nabla u \rrbracket = \llbracket w \rrbracket = 0 \quad \text{at } \mathbf{x}_\Gamma(\mathbf{x}) \in \Gamma.$$

Consequently, the contribution of Nitsche integrals to the weak form vanishes if the jumps do.

A diffuse interface counterpart of the sharp interface formulation (9) is given by (cf. [20])

$$\begin{aligned} & \int_{\Omega_{h,1}(\delta)} \mu_1((1 + H(\phi))\nabla u_{h,1} - \mathbf{g}_{h,1}) \cdot \nabla w_{h,1} \, d\mathbf{x} - \int_\Omega \mathcal{E}_{\text{cp}}q_1(u_{h,1}, u_{h,2}, w_{h,1}) \delta_\epsilon(\phi) |\nabla\phi| \, d\mathbf{x} \\ & + \int_{\Omega_{h,2}(\delta)} \mu_2((2 - H(\phi))\nabla u_{h,2} - \mathbf{g}_{h,2}) \cdot \nabla w_{h,2} \, d\mathbf{x} + \int_\Omega \mathcal{E}_{\text{cp}}q_2(u_{h,1}, u_{h,2}, w_{h,2}) \delta_\epsilon(\phi) |\nabla\phi| \, d\mathbf{x} \\ & = \int_{\Omega_1} f_1 w_{h,1} \, d\mathbf{x} + \int_{\Omega_2} f_2 w_{h,2} \, d\mathbf{x} \quad \forall \{w_{h,1}, w_{h,2}\} \in V_{h,1}(\delta) \times V_{h,2}(\delta). \end{aligned}$$

In the numerical examples of Section 6, we define $\delta_\epsilon(\phi)$ using the Gaussian regularization

$$\delta_\epsilon(\phi) = H'_\epsilon(x) = \frac{1}{\epsilon} \sqrt{\frac{\pi}{9}} \exp\left(\frac{-\pi^2 \phi^2}{9\epsilon^2}\right), \quad H_\epsilon(\phi) = \frac{1}{2} \left(1 + \operatorname{erf}\left(\frac{\pi\phi}{3\epsilon}\right)\right), \quad (10)$$

where $\operatorname{erf}(x) = \frac{2}{\sqrt{\pi}} \int_0^x e^{-y^2} \, dy$ is the Gauss error function and $H_\epsilon(\phi)$ is a smooth approximation to the sharp Heaviside function $H(\phi)$.

Remark 2. For $\delta = \operatorname{diam}(\bar{\Omega})$, which is a valid choice, the extended subdomains $\Omega_{h,k}(\delta)$, $k = 1, 2$ coincide with Ω , and the spaces $V_{h,k}(\delta)$, $k = 1, 2$ coincide with the FE space for the whole domain. This version of the diffuse-interface GP method is particularly easy to implement in an existing finite element code because it boils down to solving two coupled subproblems on the same mesh.

5. Analysis of the GP stabilization

In this section, we analyze the sharp interface formulation (9) of our unfitted finite element method and prove several useful properties of the gradient-penalty stabilization. For the purpose of analysis, we assume that the mesh is shape regular and quasiuniform. Furthermore, we assume that $\delta \leq Ch$, where δ is the extension width and $C \geq 0$ is an $O(1)$ constant. For brevity, we drop δ in the notation for the extended domains and finite element spaces below.

We define the operator $\mathcal{P}_k : (L^2(\Omega_{h,k}))^d \rightarrow (V_{h,k})^d$ for vector fields $\mathbf{v} \in (L^2(\Omega_{h,k}))^d$ as follows:

$$\mathcal{P}_k \mathbf{v} = \sum_{j=1}^{N_{h,k}} \mathbf{g}_{j,k}(\mathbf{v}) \varphi_j, \quad \mathbf{g}_{j,k}(\mathbf{v}) = \frac{\int_{\Omega_{h,k}} \mathbf{v} \varphi_j \, d\mathbf{x}}{\int_{\Omega_{h,k}} \varphi_j \, d\mathbf{x}}, \quad k = 1, 2. \quad (11)$$

The bilinear form (7) of the GP stabilization term uses $\mathbf{g}_{h,k} = \mathcal{P}_k \nabla u_k$ and can be written as

$$s_h(u, v) = \sum_{k=1}^2 s_{h,k}(u_k, v_h), \quad s_{h,k}(u, v) = \int_{\Omega_{h,k}} (\nabla u - \mathcal{P}_k \nabla u) \cdot \nabla v \, d\mathbf{x}, \quad u, v \in H^1(\Omega_{h,k}). \quad (12)$$

We shall write $a \lesssim b$ if $a \leq cb$ holds with a constant c that may depend only on the shape regularity of the mesh but not on discretization parameter h or the position of the interface Γ in the background mesh. We write $a \simeq b$ if both $a \lesssim b$ and $b \lesssim a$ hold. We first prove the following result.

Lemma 1. *The bilinear form $s_{h,k}(u, v)$ is symmetric. Furthermore, the following equivalence holds*

$$s_{h,k}(u, u) \simeq \|\nabla u - \mathcal{P}_k(\nabla u)\|_{L^2(\Omega_{h,k})}^2 + h^2 \|\nabla \mathcal{P}_k(\nabla u)\|_{L^2(\Omega_{h,k})}^2 \quad \forall u \in H^1(\Omega_{h,k}). \quad (13)$$

Proof. Let $M = (M_{ij})_{i,j=1}^N$ be the finite element mass matrix (Gram matrix) corresponding to the nodal basis of the space $V_{h,k}$. Denote by \widetilde{M} the lumped mass matrix, i.e., a diagonal matrix with $\widetilde{M}_{ii} = \sum_{j=1}^N M_{ij}$. Note that $M_{ij} \geq 0$ for linear Lagrange finite elements and that

$$\mathbf{w}^T (\widetilde{M} - M) \mathbf{w} = \sum_{i=1}^N \sum_{j=i+1}^N M_{ij} (\mathbf{w}_i - \mathbf{w}_j)^2 \quad \forall \mathbf{w} \in \mathbb{R}^N \quad (14)$$

holds by definition of M and \widetilde{M} . It follows that the matrix $\widetilde{M} - M$ is positive semi-definite.

For $w, v \in V_{h,k}$, we denote by $\mathbf{w}, \mathbf{v} \in \mathbb{R}^N$ the corresponding vectors of coefficients in the Lagrange basis of $V_{h,k}$. The result below follows from (14) and is well known (see, e.g., [3, Proposition 1]):

$$c_0 \sum_{K \in \mathcal{T}_{h,k}} h_K^2 \|\nabla w\|_{L^2(K)}^2 \leq \mathbf{w}^T (\widetilde{M} - M) \mathbf{w} \leq C_0 \sum_{K \in \mathcal{T}_{h,k}} h_K^2 \|\nabla w\|_{L^2(K)}^2, \quad (15)$$

where $h_K = \text{diam}(K)$ and $C_0, c_0 > 0$ are constants depending only on the shape regularity of the mesh.

A ‘lumped’ L^2 inner product is defined by

$$(w_h, v_h)_\ell := \mathbf{w}^T \widetilde{M} \mathbf{v}.$$

It is easy to verify that \mathcal{P}_k satisfies the identity

$$(\phi_h, \mathcal{P}_k g)_\ell = (\phi_h, g)_{L^2(\Omega_{h,k})} \quad \forall \phi_h \in V_{h,k}, \quad g \in L^2(\Omega_{h,k}). \quad (16)$$

Substituting the scalar components of $\phi_h = \mathcal{P}_k \nabla v$ and $\mathbf{g} = \nabla u$ into (16), we find that

$$(\mathcal{P}_k \nabla v, \mathcal{P}_k \nabla u)_\ell = (\mathcal{P}_k \nabla v, \nabla u)_{L^2(\Omega_{h,k})}. \quad (17)$$

Here and below, the inner products should be understood componentwise. Using (17), we obtain

$$\begin{aligned} s_{h,k}(u, v) &= (\nabla u - \mathcal{P}_k \nabla u, \nabla v - \mathcal{P}_k \nabla v)_{L^2(\Omega_{h,k})} + (\nabla u - \mathcal{P}_k \nabla u, \mathcal{P}_k \nabla v)_{L^2(\Omega_{h,k})} \\ &= (\nabla u - \mathcal{P}_k \nabla u, \nabla v - \mathcal{P}_k \nabla v)_{L^2(\Omega_{h,k})} + (\mathcal{P}_k \nabla v, \mathcal{P}_k \nabla u)_\ell - (\mathcal{P}_k \nabla u, \mathcal{P}_k \nabla v)_{L^2(\Omega_{h,k})}. \end{aligned}$$

This shows the symmetry of $s_{h,k}(u, v)$.

To prove (13), we show that the difference of the last two terms on the right-hand side is equivalent to $h^2 \|\nabla \mathcal{P}_k(\nabla u)\|_{L^2(\Omega_{h,k})}^2$. This follows from (15), the quasiuniformity of the mesh, and the observation that $\mathcal{P}_k \nabla u$ is an element of $(V_{h,k})^d$. Indeed, for any $w_h \in V_{h,k}$ we have the estimate

$$(w_h, w_h)_\ell - (w_h, w_h)_{L^2(\Omega_{h,k})} = \mathbf{w}^T \widetilde{M} \mathbf{w} - \mathbf{w}^T M \mathbf{w} = \mathbf{w}^T (\widetilde{M} - M) \mathbf{w} \simeq \sum_{K \in \mathcal{T}_h} h_K^2 \|\nabla w_h\|_{L^2(K)}^2,$$

which holds componentwise for $\mathbf{w}_h = \mathcal{P}_k(\nabla u_h)$. This proves (13). \square

Let us now estimate $s_{h,k}(u, u)$ from below by a sum of local stabilization forms associated with element patches. We denote by $\mathcal{F}_{h,k}$ the set of internal faces (edges in 2D) of the sub-triangulation $\mathcal{T}_{h,k}$ and let $\bar{\omega}(f) = K \cup K'$ be the union of two simplices sharing a face $f \in \mathcal{F}_{h,k}$. Using the notation $h_f = \max\{h_K, h_{K'}\}$ for the local mesh size of the patch, we define

$$s_{h,k}^f(u, v) = \int_{\omega(f)} [(\nabla u - \mathcal{P}_k \nabla u) \cdot (\nabla v - \mathcal{P}_k \nabla v)] \, d\mathbf{x} + h_f^2 \int_{\omega(f)} (\nabla \mathcal{P}_k \nabla u) : (\nabla \mathcal{P}_k \nabla v) \, d\mathbf{x}.$$

The estimate (13) implies

$$s_{h,k}(u, u) \gtrsim \sum_{f \in \mathcal{F}_{h,k}} s_{h,k}^f(u, u) \quad \forall u \in H^1(\Omega_{h,k}) \quad (18)$$

with some $c > 0$ depending only on the shape regularity of the mesh.

We are now ready to prove a key technical result.

Lemma 2. For arbitrary $K_1, K_2 \in \mathcal{T}_{h,k}$ such that $K_1 \cup K_2 = \bar{\omega}(f)$ for a face $f \in \mathcal{T}_{h,k}$, the following estimates hold

$$c_1 \|\nabla u\|_{L^2(K_2)}^2 \leq \|\nabla u\|_{L^2(K_1)}^2 + s_{h,k}^f(u, u) \quad \forall u \in H^1(\Omega_{h,k}), \quad (19)$$

$$c_0 \|u_h\|_{L^2(K_2)}^2 \leq \|u_h\|_{L^2(K_1)}^2 + h^2 s_{h,k}^f(u_h, u_h) \quad \forall u_h \in V_{h,k} \quad (20)$$

with some constants $c_0, c_1 > 0$ depending only on the shape regularity of the mesh.

Proof. By the triangle inequality, we have

$$\|\nabla u\|_{L^2(K_2)} \leq \|\nabla u - \mathcal{P}_k \nabla u\|_{L^2(K_2)} + \|\mathcal{P}_k \nabla u\|_{L^2(K_2)}. \quad (21)$$

Let $\mathbf{w}_h = \mathcal{P}_k \nabla u$. Then $\mathbf{w}_h \in (V_{h,k})^d$. Using the trace inequality and scaling arguments, we estimate the second term on the right-hand side of (21) as follows:

$$\begin{aligned} \|\mathcal{P}_k \nabla u\|_{L^2(K_2)}^2 &= \|\mathbf{w}_h\|_{L^2(K_2)}^2 \lesssim h_{K_2}^2 \|\nabla \mathbf{w}_h\|_{L^2(K_2)}^2 + h_f \|\mathbf{w}_h\|_{L^2(f)}^2 \\ &\lesssim h_{K_2}^2 \|\nabla \mathbf{w}_h\|_{L^2(K_2)}^2 + h_{K_1}^2 \|\nabla \mathbf{w}_h\|_{L^2(K_1)}^2 + \|\mathbf{w}_h\|_{L^2(K_1)}^2 \\ &\lesssim h_f^2 \|\nabla \mathcal{P}_k \nabla u\|_{\omega(f)}^2 + \|\nabla u\|_{L^2(K_1)}^2. \end{aligned}$$

Together with (21) and the definition of $s_{h,k}^f(\cdot, \cdot)$ this proves the result claimed in (19).

To prove the validity of (20), we use the finite element inverse and trace estimates, as well as (19), in the chain of estimates

$$\begin{aligned} \|u_h\|_{L^2(K_2)}^2 &\lesssim h_{K_2}^2 \|\nabla u_h\|_{L^2(K_2)}^2 + h_f \|u_h\|_{L^2(f)}^2 \\ &\leq h_{K_2}^2 c_1^{-1} (\|\nabla u_h\|_{L^2(K_1)}^2 + s_{h,k}^f(u_h, u_h)) + h_f \|u_h\|_{L^2(f)}^2 \\ &\lesssim h_{K_2}^2 s_{h,k}^f(u_h, u_h) + h_{K_1}^2 \|\nabla u_h\|_{L^2(K_1)}^2 + \|u_h\|_{L^2(K_1)}^2 \\ &\lesssim h_{K_2}^2 s_{h,k}^f(u_h, u_h) + \|u_h\|_{L^2(K_1)}^2, \end{aligned}$$

which complete the proof of the lemma. \square

Recall that $\Omega_{h,k}$ consists of simplices contained in $\bar{\Omega}_k$ and layers of simplices $K \notin \bar{\Omega}_k$ that intersect the δ -neighborhood of Γ . Because of our assumption on δ , the number of layers is finite and independent of h . Then the smoothness of $\partial\Omega$ and the regularity of the mesh imply (see, e.g., [21]) that any $K \in \mathcal{T}_h \cap \Omega_{h,k}$ can be reached from a strictly interior simplex by crossing a ‘finite’ number of faces. Moreover, the number of paths originating from any interior simplex is uniformly bounded. Using this argument, as well as the estimates (19) and (18), we find that

$$\|\nabla u\|_{L^2(\Omega_{h,k})}^2 \lesssim \|\nabla u\|_{L^2(\Omega_k)}^2 + s_{h,k}(u, u) \quad \forall u \in H^1(\Omega_{h,k}). \quad (22)$$

This coercivity result is important for performing stability and error analysis. The estimate provided by (20) is helpful for the analysis of evolving interface problems, which is not a subject of this paper.

We now proceed with the consistency analysis. Consistency results for the elliptic part and the Nitsche terms in the finite element formulation are provided by the standard theory. Therefore, we focus our attention on the new stabilization–extension term.

We first need several results regarding the stability and approximation properties of the operator \mathcal{P}_k defined in (11).

Lemma 3. *The mapping \mathcal{P}_k is both L^2 - and H^1 -stable, i.e., it has the property that*

$$\|\mathcal{P}_k v\|_{L^2(\Omega_{h,k})} \lesssim \|v\|_{L^2(\Omega_{h,k})} \quad \text{and} \quad \|\nabla \mathcal{P}_k w\|_{L^2(\Omega_{h,k})} \lesssim \|\nabla w\|_{L^2(\Omega_{h,k})} \quad (23)$$

for any $v \in L^2(\Omega_{h,k})$, $w \in H^1(\Omega_{h,k})$, $k = 1, 2$. Furthermore, it holds

$$\|v - \mathcal{P}_k v\|_{L^2(\Omega_{h,k})} \lesssim h \|\nabla v\|_{L^2(\Omega_{h,k})} \quad \forall v \in H^1(\Omega_{h,k}). \quad (24)$$

Proof. The consistent and lumped mass matrices are spectrally equivalent [28], which implies $\|\phi_h\|_\ell \lesssim \|\phi_h\|_{L^2(\Omega_{h,k})}$ for any $\phi_h \in V_{h,k}$. Using this fact and choosing $\phi_h = \mathcal{P}_k v$ in (16), we obtain

$$\|\mathcal{P}_k v\|_{L^2(\Omega_{h,k})}^2 \lesssim \|\mathcal{P}_k v\|_\ell^2 = (\mathcal{P}_k v, v)_{L^2(\Omega_{h,k})} \leq \|\mathcal{P}_k v\|_{L^2(\Omega_{h,k})} \|v\|_{L^2(\Omega_{h,k})}.$$

This implies the first inequality in (23).

In the next step, we first check the validity of (24) assuming that $v_h \in V_{k,h} \subset H^1(\Omega_{h,k})$. In this case, due to the assumption of a quasiuniform mesh, we have

$$\begin{aligned} \|v_h - \mathcal{P}_k v_h\|_{L^2(\Omega_{h,k})}^2 &\simeq h^d \sum_{j=1}^{N_{h,k}} \left[\frac{\int_{\omega(\mathbf{x}_j)} v_h \varphi_j \, d\mathbf{x}}{\int_{\omega(\mathbf{x}_j)} \varphi_j \, d\mathbf{x}} - v_h(\mathbf{x}_j) \right]^2 \\ &\simeq h^{-d} \sum_{j=1}^{N_{h,k}} \left[\int_{\omega(\mathbf{x}_j)} v_h \varphi_j \, d\mathbf{x} - v_h(\mathbf{x}_j) \int_{\omega(\mathbf{x}_j)} \varphi_j \, d\mathbf{x} \right]^2. \end{aligned} \quad (25)$$

Here $\omega(\mathbf{x}_j)$ denotes a domain consisting of simplices that share the grid node \mathbf{x}_j . By a standard argument that involves a pullback to a reference triangle, using a norm equivalence and a pushforward, one can show that for any $K \in \mathcal{T}_h$ and a grid node $\mathbf{x}_j \in K$ the following estimate holds:

$$\left| \int_K v_h \varphi_j \, d\mathbf{x} - v_h(\mathbf{x}_j) \int_K \varphi_j \, d\mathbf{x} \right| \lesssim h \|\nabla v_h\|_{L^2(K)} \|\varphi_j\|_{L^2(K)}.$$

Summing up over all simplices from $\omega(\mathbf{x}_j)$ and noting that $\|\varphi_j\|_{L^2(\omega(\mathbf{x}_j))} \simeq h^{d/2}$ gives

$$\left| \int_{\omega(\mathbf{x}_j)} v_h \varphi_j \, d\mathbf{x} - v_h(\mathbf{x}_j) \int_{\omega(\mathbf{x}_j)} \varphi_j \, d\mathbf{x} \right| \lesssim h^{d/2+1} \|\nabla v_h\|_{L^2(\omega(\mathbf{x}_j))}.$$

Substituting this estimate into the right hand side of (25) proves (24) for $v_h \in V_{k,h}$. To extend (24) to arbitrary $v \in H^1(\Omega_{h,k})$, we consider the L^2 -orthogonal projection $\mathcal{Q}_h v \in V_{k,h}$ and apply the triangle inequality to obtain an upper bound for

$$\|v - \mathcal{P}_k v\|_{L^2(\Omega_{h,k})} \leq \|\mathcal{P}_k(\mathcal{Q}_h v - v)\|_{L^2(\Omega_{h,k})} + \|\mathcal{P}_k(\mathcal{Q}_h v) - \mathcal{Q}_h v\|_{L^2(\Omega_{h,k})} + \|v - \mathcal{Q}_h v\|_{L^2(\Omega_{h,k})}.$$

We then use the L^2 -stability of \mathcal{P}_k , estimate (24) on $V_{k,h}$, as well as the H^1 -stability and approximation properties of the L^2 -orthogonal projection on quasiuniform meshes to show that the right hand side is bounded by $h\|\nabla v\|_{L^2(\Omega_{h,k})}$, which proves that (24) is valid for all $v \in H^1(\Omega_{h,k})$.

The second estimate in (23) can now be deduced using the triangle inequality, the finite element inverse inequality, (24), as well as the H^1 -stability and approximation properties of the L^2 -orthogonal projection:

$$\begin{aligned} \|\nabla \mathcal{P}_k v\|_{L^2(\Omega_{h,k})} &\leq \|\nabla(\mathcal{P}_k v - \mathcal{Q}_h v)\|_{L^2(\Omega_{h,k})} + \|\nabla \mathcal{Q}_h v\|_{L^2(\Omega_{h,k})} \\ &\lesssim h^{-1}\|\mathcal{P}_k v - \mathcal{Q}_h v\|_{L^2(\Omega_{h,k})} + \|\nabla v\|_{L^2(\Omega_{h,k})} \\ &\lesssim h^{-1}\|\mathcal{P}_k v - v\|_{L^2(\Omega_{h,k})} + h^{-1}\|v - \mathcal{Q}_h v\|_{L^2(\Omega_{h,k})} + \|\nabla v\|_{L^2(\Omega_{h,k})} \\ &\lesssim \|\nabla v\|_{L^2(\Omega_{h,k})}. \end{aligned}$$

□

Next, we prove the following continuity and consistency result for the GP stabilization operator.

Lemma 4. *There holds*

$$s_{h,k}(u, v) \lesssim \|u\|_{H^1(\Omega_{h,k})}\|v\|_{H^1(\Omega_{h,k})} \quad \forall u, v \in H^1(\Omega_{h,k}), v \in H^1(\Omega_{h,k}), \quad (26)$$

$$s_{h,k}(u, u) \lesssim h^2\|u\|_{H^2(\Omega_{h,k})}^2 \quad \forall u \in H^2(\Omega_{h,k}). \quad (27)$$

Proof. The continuity estimate (26) follows from the Cauchy–Schwarz inequality and the L^2 -stability of \mathcal{P}_k :

$$\begin{aligned} s_{h,k}(u, v) &= \int_{\Omega_{h,k}} (\nabla u - \mathcal{P}_k \nabla u) \cdot \nabla v \, dx \leq \|\nabla u - \mathcal{P}_k \nabla u\|_{L^2(\Omega_{h,k})} \|\nabla v\|_{L^2(\Omega_{h,k})} \\ &\leq (\|\nabla u\|_{L^2(\Omega_{h,k})} + \|\mathcal{P}_k \nabla u\|_{L^2(\Omega_{h,k})}) \|\nabla v\|_{L^2(\Omega_{h,k})} \lesssim \|u\|_{H^1(\Omega_{h,k})} \|v\|_{H^1(\Omega_{h,k})}. \end{aligned}$$

To verify (27), we employ (13), the H^1 stability of \mathcal{P}_k and (24):

$$s_{h,k}(u, u) \lesssim \|\nabla u - \mathcal{P}_k(\nabla u)\|_{L^2(\Omega_{h,k})}^2 + c h^2 \|\nabla \mathcal{P}_k(\nabla u)\|_{L^2(\Omega_{h,k})}^2 \lesssim h^2 \|\nabla^2 u\|_{L^2(\Omega_{h,k})}^2.$$

□

To formulate a convergence result, we need the following norm

$$\|v\|_*^2 = \sum_{k=1}^2 \left\{ \|v_k\|_{H^1(\Omega_{h,k})}^2 + h^{-1} \|v_k\|_{L^2(\Gamma)}^2 + s_{h,k}(v_k, v_k) \right\} \quad \text{for } v \in H^1(\Omega_{h,1}) \times H^1(\Omega_{h,2}).$$

If $u_k \in H^1(\Omega_k)$, there exists a bounded linear operator $\mathcal{E} = \mathcal{E}_k : H^1(\Omega_k) \rightarrow H^1(\mathbb{R}^d)$ that extends u_k to $\mathcal{E}u_k \in H^1(\Omega)$. Moreover, \mathcal{E}_k is also bounded as an operator from $H^2(\Omega_k)$ to $H^2(\mathbb{R}^d)$; see [25]. Whenever this causes no confusion, we will identify u_k with its extension $\mathcal{E}u_k$ to Ω .

Assume that $u \in H^2(\Omega_1) \times H^2(\Omega_2)$ solves problem (1). We associate with u its double-extension $\mathcal{E}u = \{\mathcal{E}u_1, \mathcal{E}u_2\}$. The theorem below proves the main convergence result.

Theorem 1. *Let u_h be a solution to (9). Then*

$$h\|u - u_h\|_* + \|u - u_h\|_{L^2(\Omega)} \lesssim h^2 \sum_{k=1}^2 \|u\|_{H^2(\Omega_k)}. \quad (28)$$

Proof. Let I_k denote the nodal interpolation operator for $\Omega_{h,k}$ and $I_h(u) \in V_{h,1} \times V_{h,2}$ the componentwise nodal interpolant of u , i.e., $I_h(u) = \{I_1(\mathcal{E}u_1), I_2(\mathcal{E}u_2)\}$. Owing to (22), one can follow standard arguments (see, e.g., [12, 7, 8]) to check that the bilinear form

$$A_h(u, v) := a(u, v) + s_h(u, v)$$

is uniformly coercive on the finite element space with respect to the $\|\cdot\|_*$ norm. We therefore have

$$\begin{aligned} \|I_h(u) - u_h\|_*^2 &\lesssim A_h(I_h(u) - u_h, I_h(u) - u_h) \\ &= a(I_h(u) - u_h, I_h(u) - u_h) + s_h(I_h(u) - u_h, I_h(u) - u_h). \end{aligned}$$

Using (26), a continuity estimate for the bilinear form $a(\cdot, \cdot)$, interpolation error estimates, and the H^2 boundedness of the extension operator \mathcal{E} , we find

$$\|I_h(u) - u_h\|_* \lesssim h \sum_{k=1}^2 \|\mathcal{E}u\|_{H^2(\Omega_{h,k})} \lesssim h \sum_{k=1}^2 \|u\|_{H^2(\Omega_k)}. \quad (29)$$

This estimate, the triangle inequality, and interpolation properties prove the first bound in (28).

We now proceed with a duality argument and consider the solution to the problem

$$\begin{aligned} -\nabla \cdot (\mu \nabla z) &= u - u_h \quad \text{in } \Omega, \\ z &= 0 \quad \text{on } \partial\Omega, \\ \llbracket z \rrbracket &= 0 \quad \text{on } \Gamma, \\ \llbracket \mu \nabla z \rrbracket &= 0 \quad \text{on } \Gamma. \end{aligned} \quad (30)$$

It is well known [17] that $z \in H^2(\Omega_1) \times H^2(\Omega_2)$ and

$$\sum_{k=1}^2 \|z\|_{H^2(\Omega_k)} \lesssim \|u - u_h\|_{L^2(\Omega)}. \quad (31)$$

Denote by $I_h(z) \in V_{h,1} \times V_{h,2}$ the componentwise nodal interpolant for (the extension of) z . Testing the first equation in (30) by $u - u_h$, integrating by parts, and utilizing (9) one finds the relation

$$\|u - u_h\|_{L^2(\Omega)}^2 = a(u - u_h, z - I_h(z)) + s_h(u_h, I_h(z)).$$

Note that due to symmetry and (13), the bilinear form $s_h(\cdot, \cdot)$ defines a semi-inner product. We use this property below to apply the Cauchy–Schwarz and triangle inequalities. Exploiting the continuity, the interpolation properties of $I_h(z)$ and (31), we arrive at

$$\begin{aligned} \|u - u_h\|_{L^2(\Omega)}^2 &\lesssim \|u - u_h\|_* \|z - I_h(z)\|_* + s_h^{\frac{1}{2}}(u_h, u_h) s_h^{\frac{1}{2}}(I_h(z), I_h(z)) \\ &\lesssim h \|u - u_h\|_* \|u - u_h\|_{L^2(\Omega)} + s_h^{\frac{1}{2}}(u_h, u_h) s_h^{\frac{1}{2}}(I_h(z), I_h(z)). \end{aligned} \quad (32)$$

This result and the estimate (28) for $\|u - u_h\|_*$ imply that

$$\begin{aligned} \|u - u_h\|_{L^2(\Omega)}^2 &\lesssim \|u - u_h\|_* \|z - I_h(z)\|_* + s_h^{\frac{1}{2}}(u_h, u_h) s_h^{\frac{1}{2}}(I_h(z), I_h(z)) \\ &\lesssim h^4 \sum_{k=1}^2 \|u\|_{H^2(\Omega_k)}^2 + s_h^{\frac{1}{2}}(u_h, u_h) s_h^{\frac{1}{2}}(I_h(z), I_h(z)). \end{aligned}$$

We estimate the last term using the triangle inequalities (26) and (27) to deduce

$$s_h^{\frac{1}{2}}(u_h, u_h) \lesssim \|u - u_h\|_* + h \sum_{k=1}^2 \|u\|_{H^2(\Omega_{h,k})} \quad (33)$$

and

$$\begin{aligned} s_h^{\frac{1}{2}}(I_h(z), I_h(z)) &\leq s_h^{\frac{1}{2}}(I_h(z) - z, I_h(z) - z) + s_h^{\frac{1}{2}}(z, z) \\ &\lesssim \sum_{k=1}^2 (\|I_h(z) - z\|_{H^1(\Omega_{h,k})} + h \|z\|_{H^2(\Omega_{h,k})}) \\ &\lesssim h \sum_{k=1}^2 \|z\|_{H^2(\Omega_{h,k})} \lesssim h \sum_{k=1}^2 \|z\|_{H^2(\Omega_k)} \\ &\lesssim h \|u - u_h\|_{L^2(\Omega)}, \end{aligned}$$

where the last two estimates follow from the boundedness of the extension operator \mathcal{E} in H^2 and from the stability result (31), respectively.

Collecting the estimates (32)–(33) proves that (28) holds for the L^2 norm of the error. \square

6. Test problems and numerical results

In this section, we perform numerical studies of our unfitted FEM with global gradient-penalty stabilization for the elliptic interface problem (1) in two space dimensions. In our numerical experiments, we consider different choices of diffusion coefficients μ , right hand sides f , and boundary conditions. The L^2 error of an unfitted finite element approximation in a domain Ω is given by

$$\|u_h - u\|_{0,\Omega} = \sqrt{\int_{\Omega} (H(\phi)u_{h,1} + (1 - H(\phi))u_{h,2} - u)^2 \, dx}. \quad (34)$$

Computations for all test cases are performed using a C++ implementation of the methods under investigation in the open-source finite element library MFEM [1, 2]. The numerical solutions are visualized using the open-source software GLVIS [11].

6.1. Poisson problem with a straight interface and a smooth solution

To begin, we apply the proposed methods to a quasi-1D version of problem (1) with a straight interface and a smooth solution. Let $\Omega = (0, 1)^2$ and $\Gamma = \{(x, y) \in \bar{\Omega} : x = 0.51\}$. The two subdomains are given by $\Omega_1 = \{(x, y) \in \Omega : x < 0.51\}$ and $\Omega_2 = \{(x, y) \in \Omega : x > 0.51\}$. We set $\mu_1 = 10^{-8}$, $\mu_2 = 1$ and $f_1 = 2 \cdot 10^{-8}$, $f_2 = 2$ in this test. The Dirichlet boundary conditions imposed at points $(x, y) \in \partial\Omega$ with $x = 0$ or $x = 1$ correspond to the analytical solution

$$u_1(x, y) = (x - 0.01)(1.01 - x) = u_2(x, y).$$

At points $(x, y) \in \partial\Omega$ with $y = 0$ or $y = 1$, we impose homogeneous Neumann boundary conditions.

Since the above exact solution is smooth and independent of y , we call this numerical experiment the smooth quasi-1D test. We performed grid convergence studies for both sharp and diffuse interface versions of our unfitted Nitsche method with GP stabilization. In particular, we studied the sensitivity of numerical results to the subdomains overlap δ . The sharp interface simulations were run with $\delta = 0$ and $\delta = 6h$. The diffuse interface method was tested for $\delta = 6h$ and $\delta = d_\Omega$, where $d_\Omega = \text{diam}(\bar{\Omega})$. For comparison purposes, we ran the same simulation with the Hansbo & Hansbo (H^2) method [12], which is essentially the FE formulation (2). The L^2 errors and experimental orders of convergence (EOC) on uniform grids are listed in Table 1. In addition, we tested the sharp interface version with $\delta = 6h$ on successively refined quasi-uniform grids, the coarsest of which is shown in Fig. 1. The L^2 error behavior is summarized in Table 2. In all cases, we observe approximately second order convergence and (almost) no dependence on the value of δ . The numerical solutions obtained on the uniform grid with $h = \frac{1}{1024}$ are shown in Fig. 2. As expected, a smooth transition from u_1 to u_2 can be observed across the interface.

| h^{-1} | H^2 | EOC | sharp $\delta = 0$ | EOC | sharp $\delta = 6h$ | EOC | diffuse $\delta = 0$ | EOC | diffuse $\delta = d_\Omega$ | EOC |
|----------|----------|------|-----------------------|------|------------------------|------|-------------------------|------|--------------------------------|------|
| 128 | 1.03e-05 | | 4.02e-05 | | 4.02e-05 | | 4.02e-05 | | 4.02e-05 | |
| 256 | 2.59e-06 | 1.99 | 1.01e-05 | 1.99 | 1.01e-05 | 1.99 | 1.01e-05 | 1.99 | 1.01e-05 | 1.99 |
| 512 | 6.48e-07 | 2.00 | 2.54e-06 | 1.99 | 2.54e-06 | 1.99 | 2.54e-06 | 1.99 | 2.54e-06 | 1.99 |
| 1024 | 1.62e-07 | 2.00 | 6.35e-07 | 2.00 | 6.35e-07 | 2.00 | 6.35e-07 | 2.00 | 6.35e-07 | 2.00 |
| 2048 | 4.05e-08 | 2.00 | 1.59e-07 | 2.00 | 1.59e-07 | 2.00 | 1.59e-07 | 2.00 | 1.59e-07 | 2.00 |
| 4096 | 9.55e-09 | 2.08 | 3.96e-08 | 2.01 | 3.99e-08 | 1.99 | 3.98e-08 | 2.00 | 3.99e-08 | 1.99 |

Table 1: Smooth quasi-1D test, L^2 convergence history on uniform meshes.

6.2. Poisson problem with a straight interface and a non-smooth solution

In our second example, the domain and interface are the same as in the quasi-1D test of Section 6.1. Following Hansbo and Hansbo [12], we set $\mu_1 = 0.5$, $\mu_2 = 3$ and $f_1 = f_2 = 1$. The Dirichlet boundary

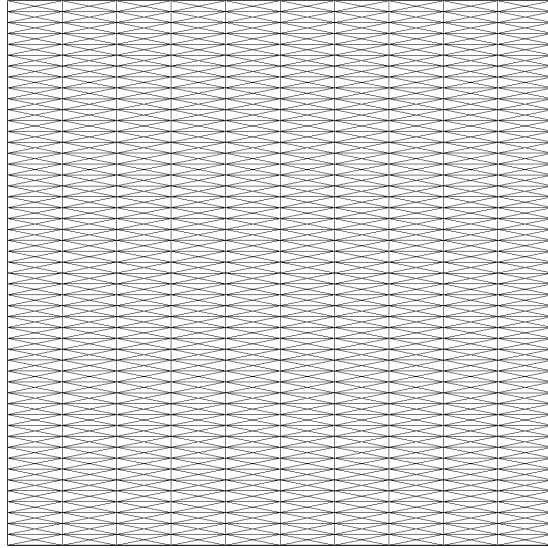


Figure 1: Coarse quasi-uniform mesh with $\Delta x = 0.1$ and $\Delta y = 0.02$.

conditions at points $(x, y) \in \partial\Omega$ with $x = 0$ or $x = 1$ are chosen to match the values of

$$u_1(x, y) = \frac{9}{14}(x - 0.01) - (x - 0.01)^2, \quad u_2(x, y) = \frac{5}{84} + \frac{9}{84}(x - 0.01) - \frac{1}{6}(x - 0.01)^2.$$

As before, we impose homogenous Neumann boundary conditions at $(x, y) \in \partial\Omega$ with $y = 0$ or $y = 1$.

The analytical solution $u(x, y)$ to this test problem coincides with $u_1(x, y)$ for $x \leq 0.51$ and with $u_2(x, y)$ for $x \geq 0.51$. Since $u(x, y)$ has a kink at $x = 0.51$, we call this experiment the non-smooth quasi-1D test. We ran grid convergence studies for the same configurations as in the previous example. The L^2 errors and EOCs for uniform meshes are listed in Table 3. Additionally, we present the L^2 convergence history for quasi-uniform meshes in Table 2. Again, we observe second order convergence and no dependence on δ for all cases. The numerical solutions obtained with $h = \frac{1}{1024}$ are shown in Fig. 3. The solutions for u_1 and u_2 match well on the interface and no oscillations occur.

Remark 3. The reported convergence behavior can be further improved by using problem-dependent values of the Nitsche parameter α . Numerical tests indicate that more stable EOCs can often be obtained by increasing or decreasing the value of α .

6.3. Poisson problem with a circular interface

Let us now apply our GP method to a truly two-dimensional test problem with a circular interface. The domain is given by $\Omega = (-1, 1)^2$. The interface Γ is the zero level set of the signed distance

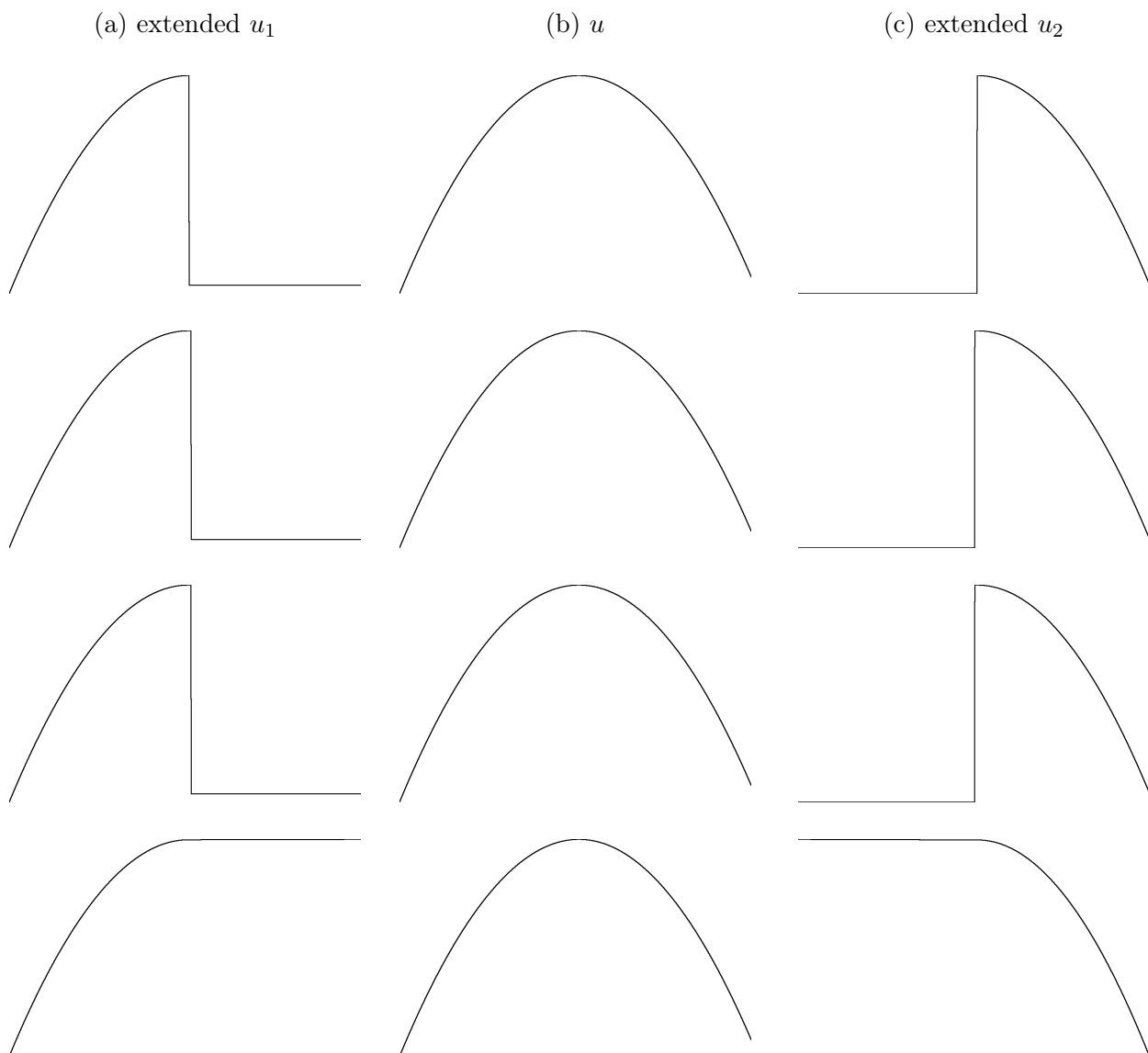


Figure 2: Numerical solutions to the smooth quasi-1D test problem (uniform mesh, $h = \frac{1}{1024}$). First row: sharp, $\delta = 0$. Second row: sharp, $\delta = 6h$. Third row: diffuse, $\delta = 6h$. Fourth row: diffuse, $\delta = d_\Omega$.

function $\phi(x, y) = 0.75 - \sqrt{x^2 + y^2}$. We set $\mu_1 = 1$, $\mu_2 = 10^3$ and $f_1 = f_2 = 4$ in this test. The Dirichlet boundary condition for points $(x, y) \in \partial\Omega$ is chosen in such a way that the restrictions

$$u_1(x, y) = x^2 - y^2, \quad u_2(x, y) = \frac{x^2 - y^2}{1000} - \frac{0.5625}{1000} + 0.5625$$

| h^{-1} | smooth | EOC | non-smooth | EOC |
|----------|----------|------|------------|------|
| 10 | 4.23e-03 | | 3.09e-03 | |
| 20 | 1.15e-03 | 1.88 | 8.36e-04 | 1.89 |
| 40 | 2.98e-04 | 1.94 | 2.16e-04 | 1.95 |
| 80 | 7.60e-05 | 1.98 | 5.50e-05 | 1.97 |
| 160 | 1.92e-05 | 1.98 | 1.39e-05 | 1.98 |
| 320 | 4.82e-06 | 1.99 | 3.48e-06 | 2.00 |
| 640 | 1.21e-06 | 1.99 | 8.72e-07 | 2.00 |

Table 2: Quasi-1D test problems, L^2 convergence of the sharp interface method on quasi-uniform meshes.

| h^{-1} | H^2 | EOC | sharp $\delta = 0$ | EOC | sharp $\delta = 6h$ | EOC | diffuse $\delta = 0$ | EOC | diffuse $\delta = d_\Omega$ | EOC |
|----------|----------|------|-----------------------|------|------------------------|------|-------------------------|------|--------------------------------|------|
| 128 | 7.47e-06 | | 2.91e-05 | | 2.91e-05 | | 2.67e-05 | | 2.67e-05 | |
| 256 | 1.86e-06 | 2.01 | 7.31e-06 | 1.99 | 7.31e-06 | 1.99 | 8.29e-06 | 1.69 | 8.29e-06 | 1.69 |
| 512 | 4.64e-07 | 2.00 | 1.83e-06 | 2.00 | 1.83e-06 | 2.00 | 1.38e-06 | 2.59 | 1.38e-06 | 2.59 |
| 1024 | 1.15e-07 | 2.01 | 4.57e-07 | 2.00 | 4.57e-07 | 2.00 | 4.16e-07 | 1.73 | 4.16e-07 | 1.73 |
| 2048 | 1.93e-08 | 2.57 | 1.03e-07 | 2.15 | 1.03e-07 | 2.15 | 9.79e-08 | 2.09 | 9.79e-07 | 2.09 |
| 4096 | 4.64e-09 | 2.06 | 2.29e-08 | 2.17 | 2.29e-08 | 2.17 | 2.75e-08 | 1.83 | 2.75e-08 | 1.83 |

Table 3: Non-smooth quasi-1D test, L^2 convergence history on uniform meshes.

define the analytical solution (cf. [12]).

We studied grid convergence of the sharp and diffuse interface version of our unfitted Nitsche method with GP stabilization. The parameter settings were chosen as in the previous examples. For comparison purposes, the same simulations were run with the H^2 method. The L^2 errors and EOCs are listed in Table 4. We observed second order convergence in all cases.

The numerical solutions corresponding to $h = \frac{1}{512}$ are shown in Figs. 4 and 5 for diffuse interface simulations with $\delta = 6h$ and $\delta = d_\Omega$, respectively. It can be seen that the unfitted finite element approximations to u_1 and u_2 match well on the circular interface. Moreover, no violations of the discrete maximum principle are observed in this experiment.

6.4. Stationary convection-diffusion problem with steep gradients

In our final example, we test a generalization of our diffuse interface method to the elliptic problem

$$\begin{aligned}
\mathbf{v} \cdot \nabla u - \nabla \cdot (\mu \nabla u) &= 0 \quad \text{in } \Omega_k, \quad k = 1, 2, \\
u &= g_D \quad \text{on } \partial\Omega, \\
[[u]] &= 0 \quad \text{on } \Gamma, \\
[[\mathbf{v}u - \mu \nabla u]] &= 0 \quad \text{on } \Gamma,
\end{aligned}$$

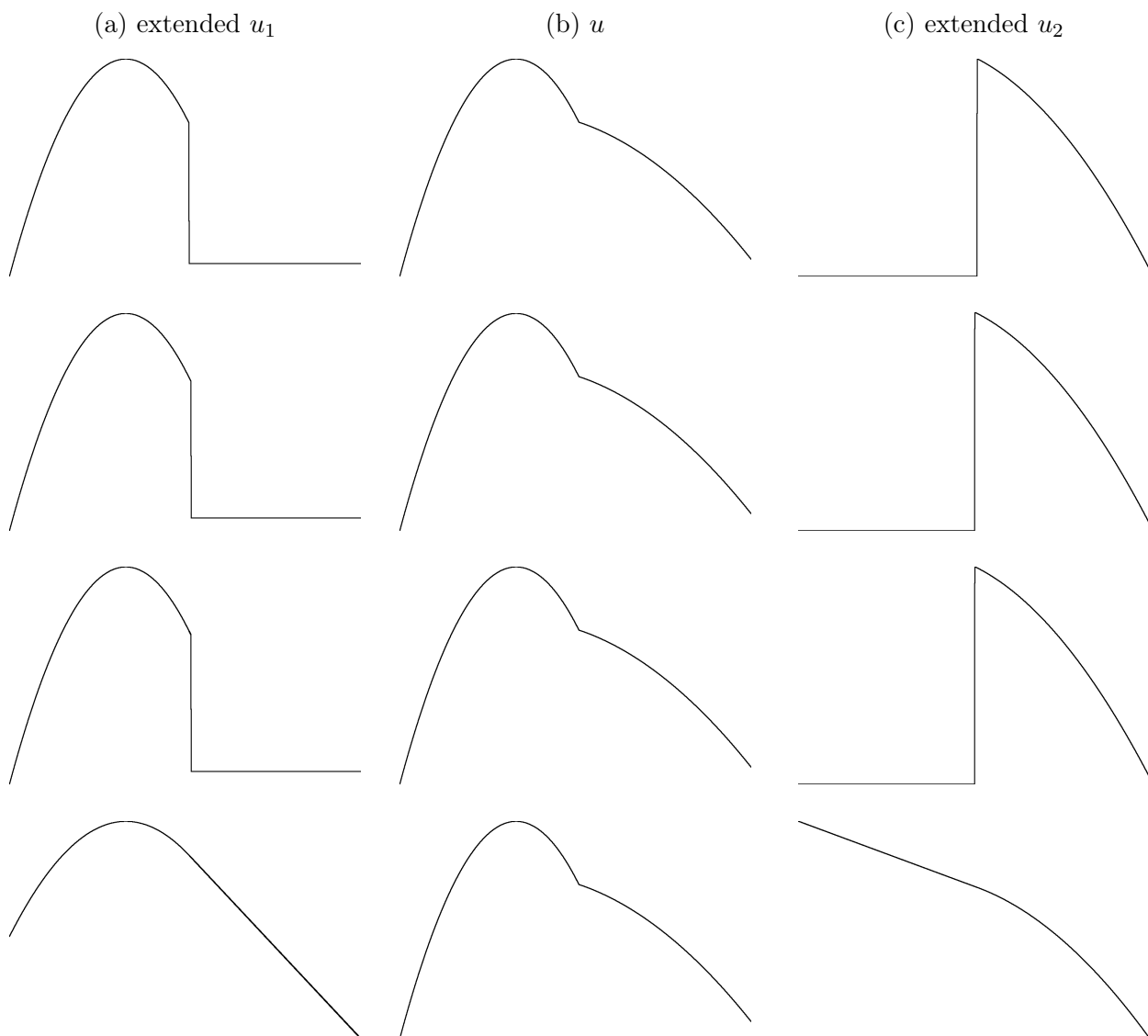


Figure 3: Numerical solutions to the non-smooth quasi-1D test problem (uniform mesh, $h = \frac{1}{256}$). First row: sharp, $\delta = 0$. Second row: sharp, $\delta = 6h$. Third row: diffuse, $\delta = 6h$. Fourth row: diffuse, $\delta = d_\Omega$.

where $\mathbf{v} \in \mathbb{R}^d$ is a constant velocity and g_D is the Dirichlet boundary data. In a corresponding straightforward extension of our diffuse interface formulation, we add the convective term

$$\mathbf{v} \cdot \left[\int_{\Omega_1} \nabla u_{h,1} w_{h,1} \, d\mathbf{x} + \int_{\Omega_2} \nabla u_{h,2} w_{h,2} \, d\mathbf{x} \right]$$

| h^{-1} | H^2 | EOC | sharp $\delta = 0$ | EOC | sharp $\delta = 6h$ | EOC | diffuse $\delta = 0$ | EOC | diffuse $\delta = d_\Omega$ | EOC |
|----------|----------|------|-----------------------|------|------------------------|------|-------------------------|------|--------------------------------|------|
| 32 | 8.62e-03 | | 1.15e-02 | | 1.17e-02 | | 9.05e-04 | | 9.74e-04 | |
| 64 | 1.86e-03 | 2.21 | 2.68e-03 | 2.10 | 2.77e-03 | 2.08 | 2.09e-04 | 2.11 | 2.44e-04 | 2.00 |
| 128 | 4.26e-04 | 2.13 | 6.59e-04 | 1.96 | 6.78e-04 | 2.03 | 5.06e-05 | 2.05 | 6.11e-05 | 2.00 |
| 256 | 9.82e-05 | 2.12 | 1.64e-04 | 2.07 | 1.69e-04 | 2.00 | 1.23e-05 | 2.04 | 1.51e-05 | 2.02 |
| 512 | 2.25e-05 | 2.13 | 4.10e-05 | 2.00 | 4.24e-05 | 1.99 | 2.96e-06 | 2.05 | 3.59e-06 | 2.07 |
| 1024 | 5.20e-06 | 2.11 | 1.04e-05 | 1.98 | 1.07e-05 | 1.99 | 6.88e-07 | 2.11 | 8.00e-07 | 2.17 |

Table 4: Circular interface test, L^2 convergence history on uniform meshes.

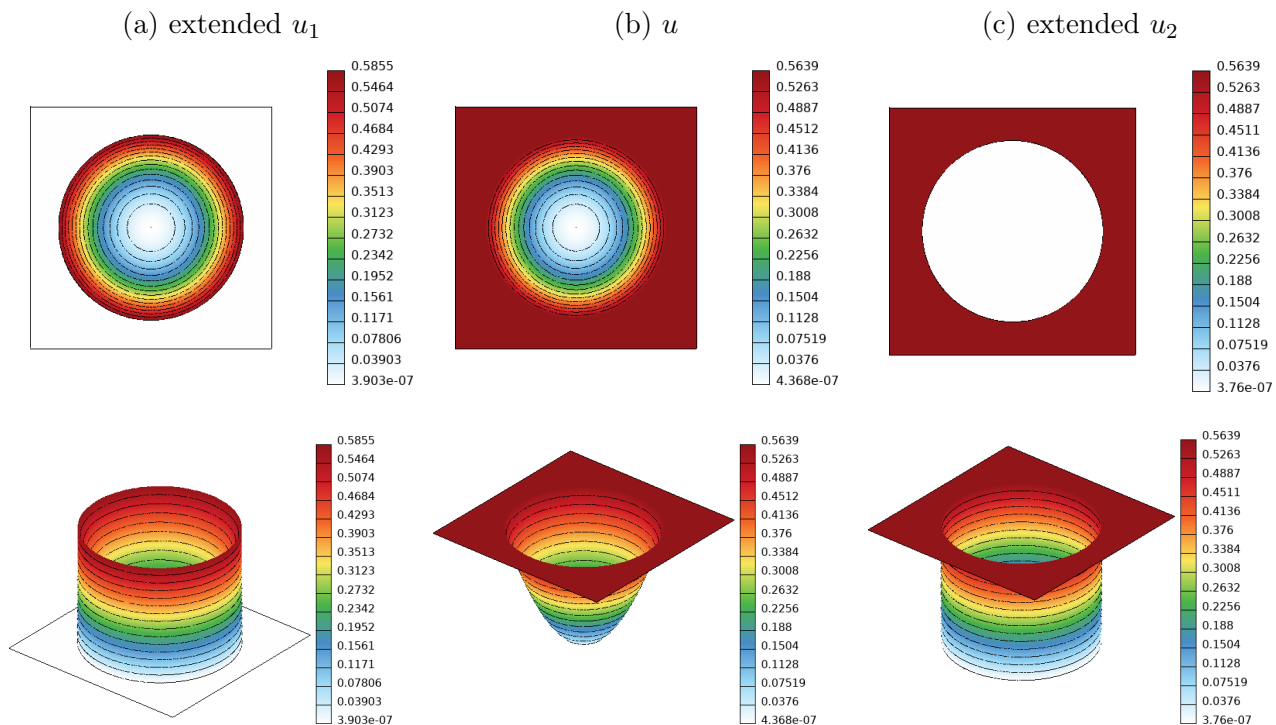


Figure 4: Numerical solutions to the circular interface test problem (uniform mesh, $h = \frac{1}{512}$, diffuse interface method, $\delta = 6h$). First row: top views. Second row: elevation is proportional to the value of the plotted function.

on the left-hand side of (10) and multiply the stabilization term $s_h(u, w)$ by (cf. [26])

$$\beta_h = \max \left\{ 1, \frac{|\mathbf{v}|h}{2\epsilon} \right\}.$$

A well-known test problem for stationary perturbed convection-diffusion equations with constant coefficients is defined in Example 2 of the review paper [16]. It uses the domain $\Omega = (0, 1)^2$ and the

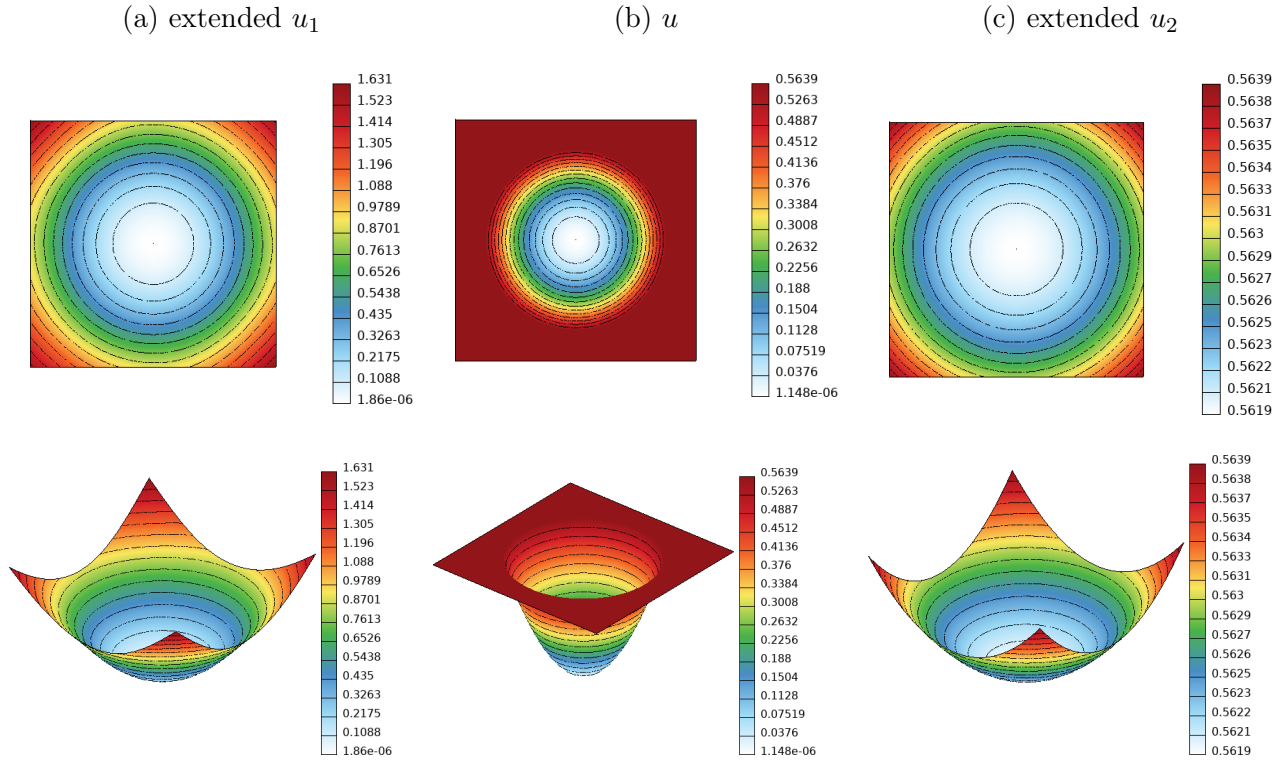


Figure 5: Numerical solutions to the circular interface test problem (uniform mesh, $h = \frac{1}{512}$, diffuse interface method, $\delta = d_\Omega$). First row: top views. Second row: elevation is proportional to the value of the plotted function.

velocity $\mathbf{v} = (\cos(-\pi/3), \sin(-\pi/3))^\top$. The Dirichlet boundary data is given by

$$g_D(x, y) = \begin{cases} 0 & \text{if } x = 1 \text{ or } y \leq 0.7, \\ 1 & \text{otherwise.} \end{cases}$$

Note that g_D is discontinuous at $(x_0, y_0) = (0, 0.7)$. Let $\Gamma = \{(x, y) \in \bar{\Omega} : ax + by = c\}$ be the straight line that passes through (x_0, y_0) and is parallel to \mathbf{v} . Deviating from the setup in [16], we set $\mu_1 = 10^{-3}$ in $\Omega_1 = \{(x, y) \in \Omega : ax + by < c\}$ and $\mu_2 = 10^{-8}$ in $\Omega_2 = \{(x, y) \in \Omega : ax + by > c\}$.

In Fig. 6, we show the numerical solutions calculated on the uniform mesh with spacing $h = \frac{1}{1024}$. It can be seen that failure to properly stabilize the discretized convective terms results in global spurious oscillations. The gradient-penalty stabilization term with the proposed choice of the parameter β_h mitigates this effect and localizes violations of the discrete maximum principle to layers of elements with steep gradients without the need for additional modifications of the discretized weak form.

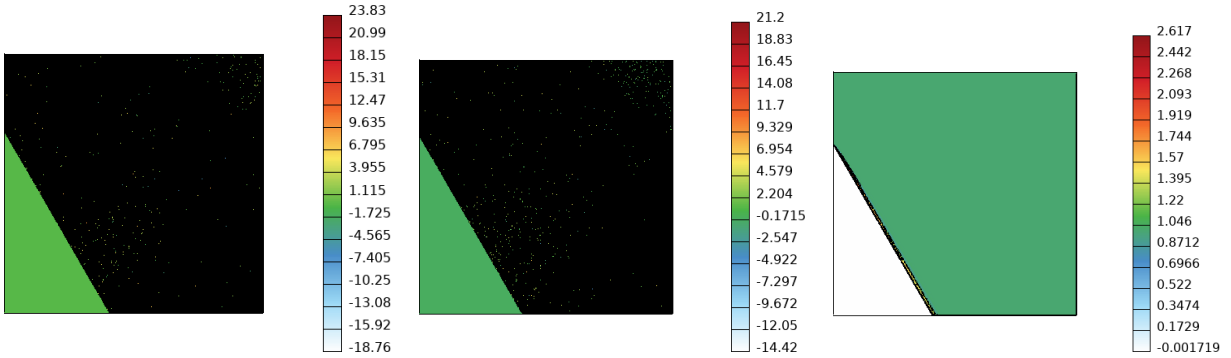


Figure 6: Numerical solutions to the stationary interface convection-diffusion problem (uniform mesh, $h = \frac{1}{1024}$, $\delta = 0$). Left: no stabilization, $\beta_h = 0$. Center: $\beta_h = 1$. Right: $\beta_h = \max \left\{ 1, \frac{|v|h}{2\epsilon} \right\}$.

7. Conclusions

The paper studied an unfitted FEM with gradient penalty stabilization. Two versions of the method, the sharp interface and diffuse interface approaches, were introduced and applied to numerically solve an elliptic interface problem. The gradient penalty stabilization was applied globally, rather than being restricted to a narrow strip around the interface.

A priori analysis of the gradient penalty stabilization was performed for the case of P^1 finite elements. The resulting sharp interface version of the FEM was proven to be optimal-order convergent. The method's performance was compared to the unstabilized variant from [12]. The proposed version demonstrated comparable accuracy while being algebraically stable, providing an extension of the solution beyond the physical domain and enabling a diffuse interface implementation. The diffuse interface variant showed similar accuracy but currently lacks numerical analysis.

We conclude that gradient penalty stabilization is a simple and effective technique that facilitates the straightforward implementation of unfitted FEM. Handling higher-order elements remains an open problem for future research.

Acknowledgments

M.O. was supported in part by the U.S. National Science Foundation under awards DMS-2309197 and DMS2408978.

References

- [1] R. Anderson, A. Barker, J. Bramwell, J.-S. Camier, J. Cervený, V. Dobrev, Y. Dudouit, A. Fisher, Tz. Kolev, W. Pazner, M. Stowell, V. Tomov, J. Dahm, D. Medina, and S. Zampini, MFEM: a modular finite element library. *Computers & Mathematics with Applications* **81** (2021) 42–74.

- [2] J. Andrej, N. Atallah, J.-P. Bäcker, J.-S. Camier, D. Copeland, V. Dobrev, Y. Dudoit, T. Duswald, B. Keith, D. Kim, T. Kolev, B. Lazarov, K. Mittal, W. Pazner, S. Petrides, S. Shiraiwa, M. Stowell and V. Tomov, High-performance finite elements with MFEM. *Int. J. of HPC Applications* **38**(5) (2024) 447–467.
- [3] R. Becker and P. Hansbo, A simple pressure stabilization method for the Stokes equation. *Commun. Numer. Methods Engrg.* (2008) 24(11):1421-30.
- [4] S.P. Bordas, E.N. Burman, M.G. Larson, and M.A. Olshanskii (Eds), Geometrically Unfitted Finite Element Methods and Applications. *Proceedings of the UCL Workshop*, Springer: LNCSE **121**, 2018.
- [5] E. Burman, Ghost penalty. *Comptes Rendus Math.* **348** (2010) 1217–1220.
- [6] E. Burman, S. Claus, and A. Massing, A stabilized cut finite element method for the three field Stokes problem. *SIAM J. Sci. Computing*, **37** (2025), A1705–A1726.
- [7] E. Burman and P. Hansbo, Fictitious domain finite element methods using cut elements: II. A stabilized Nitsche method. *Appl. Numer. Math.* **62** (2012) 328–341.
- [8] E. Burman, S. Claus, P. Hansbo, M.G. Larson, and A. Massing, CutFEM: Discretizing geometry and partial differential equations. *Int. J. Numer. Meth. Engrg.* **104** (2015) 472–501.
- [9] R. Codina and J. Blasco, A finite element formulation for the Stokes problem allowing equal velocity-pressure interpolation. *Computer Methods Appl. Mech. Engrg.* **143** (1997) 373–391.
- [10] R. Codina and J. Blasco, Analysis of a stabilized finite element approximation of the transient convection-diffusion-reaction equation using orthogonal subscales. *Comput. Visual Sci.* **4** (2002) 167–174.
- [11] GIVis: OpenGL Finite Element Visualization Tool. <https://glvis.org>
- [12] P. Hansbo and A. Hansbo, An unfitted finite element method, based on Nitsche’s method, for elliptic interface problems. *Comput. Methods Appl. Mech. Engrg.* **191** (2002) 5537–5552.
- [13] S. Hysing, A new implicit surface tension implementation for interfacial flows. *Int. J. Numer. Methods Fluids* **51** (2006) 659–672.
- [14] V. John, S. Kaya, and W. Layton, A two-level variational multiscale method for convection-dominated convection-diffusion equations. *Computer Methods Appl. Meth. Engrg.* **195** (2006) 4594–4603.
- [15] V. John and A. Kindl, A variational multiscale method for turbulent flow simulation with adaptive large scale space. *J. Comput. Phys.* **229** (2010) 301–312.

- [16] V. John and P. Knobloch, On spurious oscillations at layers diminishing (SOLD) methods for convection–diffusion equations: Part I – A review. *Comput. Methods Appl. Mech. Engrg.* **196** (2007) 2197–2215.
- [17] R. B. Kellogg, On the Poisson equation with intersecting interfaces. *Applicable Analysis*, **4**(2) (1974) 101–129.
- [18] C. Kublik and R. Tsai, Integration over curves and surfaces defined by the closest point mapping. *Res. Math. Sci.* **3** (2016) 1–17.
- [19] C. Kublik and R. Tsai, An extrapolative approach to integration over hypersurfaces in the level set framework. *Math. Comp.* **87** (2018) 2365–2392.
- [20] D. Kuzmin and J.-P. Bäcker, An unfitted finite element method using level set functions for extrapolation into deformable diffuse interfaces. *J. Comput. Phys.* **461** (2022) 111218.
- [21] C. Lehrenfeld and M. Olshanskii, An Eulerian finite element method for PDEs in time-dependent domains. *ESAIM: M2AN* **53** (2019) 585–614.
- [22] J. Nitsche, Über ein Variationsprinzip zur Lösung von Dirichlet-Problemen bei Verwendung von Teilräumen, die keinen Randbedingungen unterworfen sind. *Abh. Math. Univ. Hamburg* **36** (1971) 9–15.
- [23] A. Massing, B. Schott, and W.A. Wall, A stabilized Nitsche cut finite element method for the Oseen problem. *Computer Methods Appl. Mech. Engrg.* **328** (2018) 262–300.
- [24] M. Olshanskii and H. von Wahl, Stability of instantaneous pressures in an Eulerian finite element method for moving boundary flow problems. Preprint arXiv:2412.17657 (2024).
- [25] E. M. Stein, *Singular Integrals and Differentiability Properties of Functions*, Princeton Mathematical Series **30**, Princeton University Press, Princeton, New Jersey, 1970.
- [26] J. Vedral, A. Rupp, and D. Kuzmin, Strongly consistent low-dissipation WENO schemes for finite elements. *Appl. Numer. Math.* **210** (2025) 64–81.
- [27] E. Wadbro, S. Zahedi, G. Kreiss, and M. Berggren, A uniformly well-conditioned, unfitted Nitsche method for interface problems. *BIT Numer. Math.* **53** (2013) 791–820.
- [28] A. Wathen, Realistic eigenvalue bounds for the Galerkin mass matrix. *IMA J. Numer. Analysis* **7** (1987) 449–457.
- [29] S. Zahedi and A.K. Tornberg, Delta function approximations in level set methods by distance function extension. *J. Comput. Phys.* **229** (2010) 2199–2219.